ACS NANO
Cite This: ACS Nano XXXX, XXX, XXX–XXX
www.acsnano.org

ARTICLE

Radiation Tolerant Nanowire Array Solar Cells

Pilar Espinet-Gonzalez,[†] Enrique Barrigón,[‡] Gaute Otnes,[‡,○] Giuliano Vescovi,[§] Colin Mann,[∥] Ryan M. France,[⊥] Alex J. Welch,[†] Matthew S. Hunt,[▽] Don Walker,[∥] Michael D. Kelzenberg,[†] Ingvar Åberg,[§] Magnus T. Borgström,[‡] Lars Samuelson,[‡,§] and Harry A. Atwater*[,†]

[†]Department of Applied Physics and Materials Science, California Institute of Technology, Pasadena, California 91125, United States
[‡]Division of Solid State Physics, Lund University, Lund, SE-221 00, Sweden
[§]Sol Voltaics AB, Lund, SE-223 63, Sweden
[∥]The Aerospace Corporation, El Segundo, California 90245-4609, United States
[⊥]National Renewable Energy Laboratory, Golden, Colorado 80401, United States
[▽]The Kavli Nanoscience Institute, California Institute of Technology, Pasadena, California 91125, United States

Supporting Information

ABSTRACT: **Space power systems require photovoltaics that are lightweight, efficient, reliable, and capable of operating for years or decades in space environment. Current solar panels use planar multijunction, III−V based solar cells with very high efficiency, but their specific power (power to weight ratio) is limited by the added mass of radiation shielding (e.g., coverglass) required to protect the cells from the high-energy particle radiation that occurs in space. Here, we demonstrate that III−V nanowire-array solar cells have dramatically superior radiation performance relative to planar solar cell designs and show this for multiple cell geometries and materials, including GaAs and InP. Nanowire cells exhibit damage thresholds ranging from ∼10−40 times higher than planar control solar cells when subjected to irradiation by 100−350 keV protons and 1 MeV electrons. Using Monte Carlo simulations, we show that this improvement is due in part to a reduction in the displacement density within the wires arising from their nanoscale dimensions. Radiation tolerance, combined with the efficient optical absorption and the improving performance of nanowire photovoltaics, indicates that nanowire arrays could provide a pathway to realize high-specific-power, substrate-free, III−V space solar cells with substantially reduced shielding requirements. More broadly, the exceptional reduction in radiation damage suggests that nanowire architectures may be useful in improving the radiation tolerance of other electronic and optoelectronic devices.**

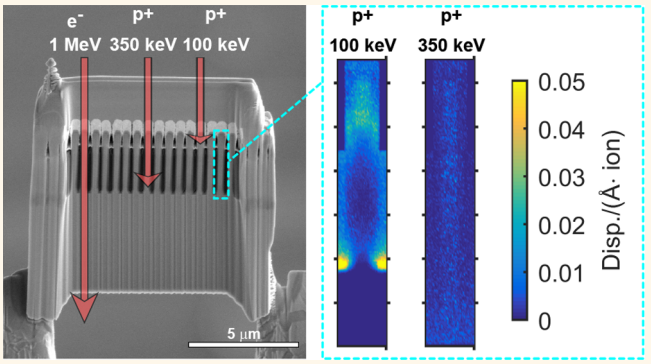

KEYWORDS: *nanowire solar cells, radiation hard, space environment, space solar cells, high specific power, irradiation-induced defects, Monte Carlo simulations*

Most spacecraft are powered by photovoltaic (PV) solar cells, which, because of the challenging space environment, are subject to stringent requirements, including high-power conversion efficiency (PCE), high reliability, high tolerance to radiation, and high specific power, that is, power-to-weight ratio. The latter requirement is crucial because the energy-generating system is typically one of the heaviest components of a satellite,[1] significantly impacting the cost of space launch. Thus, substantial efforts have been made to increase the specific power of space solar panels, while ensuring that the solar cells will produce adequate power throughout the mission duration.

In the space environment, solar panels are subject to severe thermal cycles, high UV light exposure, atomic oxygen in low earth orbit, space debris, meteoroid impact, electrostatic charging, and high energy particle radiation. Standard space solar arrays composed of III−V solar cells degrade almost exclusively by high energy electron and proton irradiation. The radiation flux, energy distribution, and fluence depend on the operating orbit, orientation of the spacecraft, solar cycle, and mission duration. Two main approaches are typically used to mitigate the detrimental effects of radiation. First, a layer of shielding (typically a cerium-doped cover glass) is used to reduce the amount of radiation reaching the solar cells but this

Received: July 2, 2019
Accepted: October 18, 2019
Published: October 18, 2019

DOI: 10.1021/acsnano.9b05213
ACS Nano XXXX, XXX, XXX–XXX

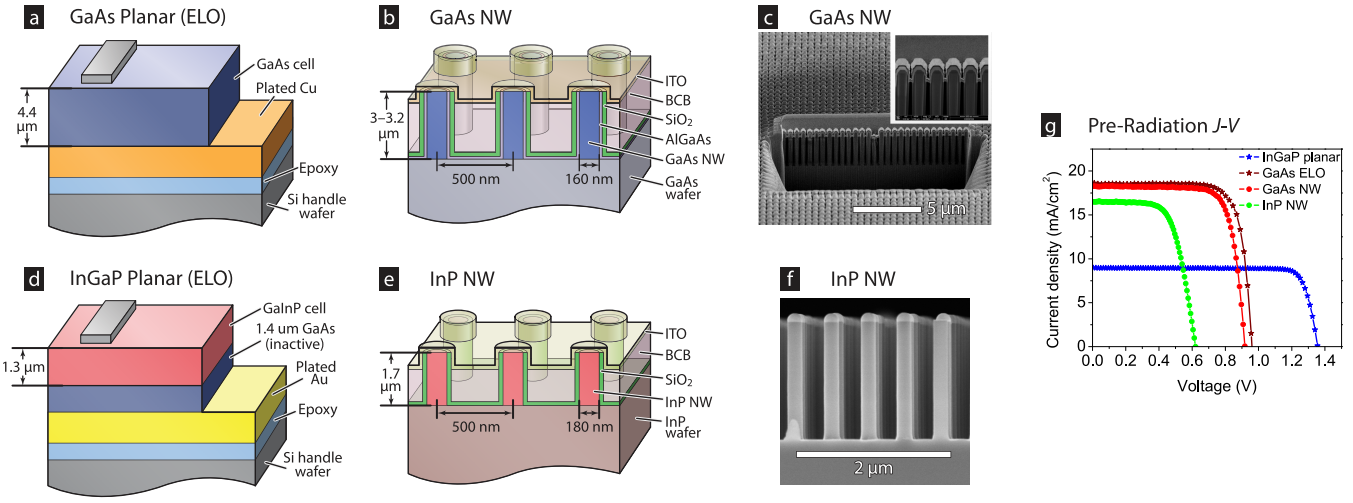

Figure 1. Schematics of all the devices tested (a,b,d,e), cross-sectional images of representative NW solar cells (c,f) and initial *J*–*V* curves of representative devices of each architecture (g). Panel c shows a completed GaAs NW solar cell, which was overcoated with metal and ion-milled to enable cross-sectional imaging. Panel f shows as-grown InP NWs with the Au growth catalyst particle still on top of the wire. In panel g, note that the planar cells lack antireflective coatings.

adds undesired weight.[2] The second approach to mitigate radiation damage is to increase the intrinsic radiation tolerance of the solar cells through choice of semiconductor materials and/or device architectures with enhanced radiation robustness, which experience less degradation for a given radiation exposure.[3−7]

State-of-the-art space solar panels composed of III−V multijunction solar cells[8,9] are attractive because of high-power conversion efficiencies (>30% under extraterrestrial solar spectrum (AM0)), enabling a reduction in the panel area for a given mission. The development of thinned-substrate[10] and epitaxial lift-off (ELO)[11] technologies have allowed extremely thin III−V solar cells to be produced, such that the mass of the panels using these cells would be dominated largely by the requisite radiation-shielding. Yet, there is a growing demand for energy conversion systems with higher specific power than can be achieved with existing technologies (that is, exceeding ∼0.2 W/g).[12] This demand is particularly driven by systems that need to operate in environments dominated by high proton fluence, such as medium earth orbit, which require heavy shielding because of the extensive exposure to radiation. Developing "rad-hard" thin-film solar cells would significantly reduce or even eliminate the need for shielding, thus maximizing the specific power.

Many photovoltaic materials systems and cell geometries have been investigated for their potentially enhanced radiation tolerance. Studies have reported radiation-tolerant thin-film solar cells based on copper indium gallium diselenide (CIGS),[13] cadmium telluride (CdTe),[14] and, more recently, perovskite compounds.[15−17] In particular, perovskite solar cells have achieved impressive specific power values exceeding 29 W/g[18] and have demonstrated outstanding radiation resistance. While promising, these thin-film technologies are substantially less efficient and less technologically mature than state-of-the-art multijunction cells and have not found widespread use in space. Within the established III−V compound semiconductor material systems, numerous approaches for radiation hardening have also been explored. Ultrathin (nanometer thickness), planar GaAs[19] has been demonstrated to reduce the short circuit current loss due to radiation damage, but thus far such cells have demonstrated a low beginning-of-life (BOL) efficiency of ∼3%. Also, GaAs solar cells with quantum dots and quantum wells have been studied as potential candidates for radiation hard devices. Quantum dots and quantum wells have been reported to have enhanced radiation tolerance[20,21] owing to their reduced effective cross section for particle-solid interactions and carrier confinement. In solar cells, the current from the quantum dots and quantum wells is significantly radiation tolerant. However, the overall radiation behavior reported in highly performing optimized quantum dots/wells solar cells is similar to standard devices.[7,22,23]

Here we propose the use of III−V nanowire (NW) arrays as space solar cell architecture with dramatically enhanced radiation tolerance versus planar architectures. The NW solar cells consist of arrays of high-aspect-ratio semiconductor structures ("wires") that have appropriate dimensions to enhance light absorption[24−27] and to reduce damage caused by high-energy particle radiation as we report here and it has been observed in photodetectors.[28−30] The NW solar cells are fabricated from the same III−V phosphide and arsenide semiconductor compounds as conventional space solar cells. Although the NW technology is less mature, in principle these cells should be capable of reaching similar high efficiencies and reliability. Reported efficiencies of NW solar cells have been rapidly increasing over the past decade, yielding values of 15.3% and 15.0% (AM1.5G) for bottom up single-junction GaAs[31] and InP[32] NW solar cells, respectively, and 17.8% for top down tapered dry-etched InP NW solar cells.[33] Furthermore, the NW growth processes can accommodate a far greater range of lattice mismatch than planar epitaxy, suggesting that defect-free multijunction cells could be grown from a diverse range of materials, to further improve the efficiency.[34−38] NW arrays have a low packing fraction (∼9−14%) and can be fabricated as devices in a substrate-free,[39−41] lightweight, flexible sheet form factor,[42−45] which is ideal for efficient packaging and deployment in space.

RESULTS AND DISCUSSION

As high energy particles pass through a semiconductor crystal, they are slowed down by interactions with electrons and atomic

DOI: 10.1021/acsnano.9b05213
ACS Nano XXXX, XXX, XXX−XXX

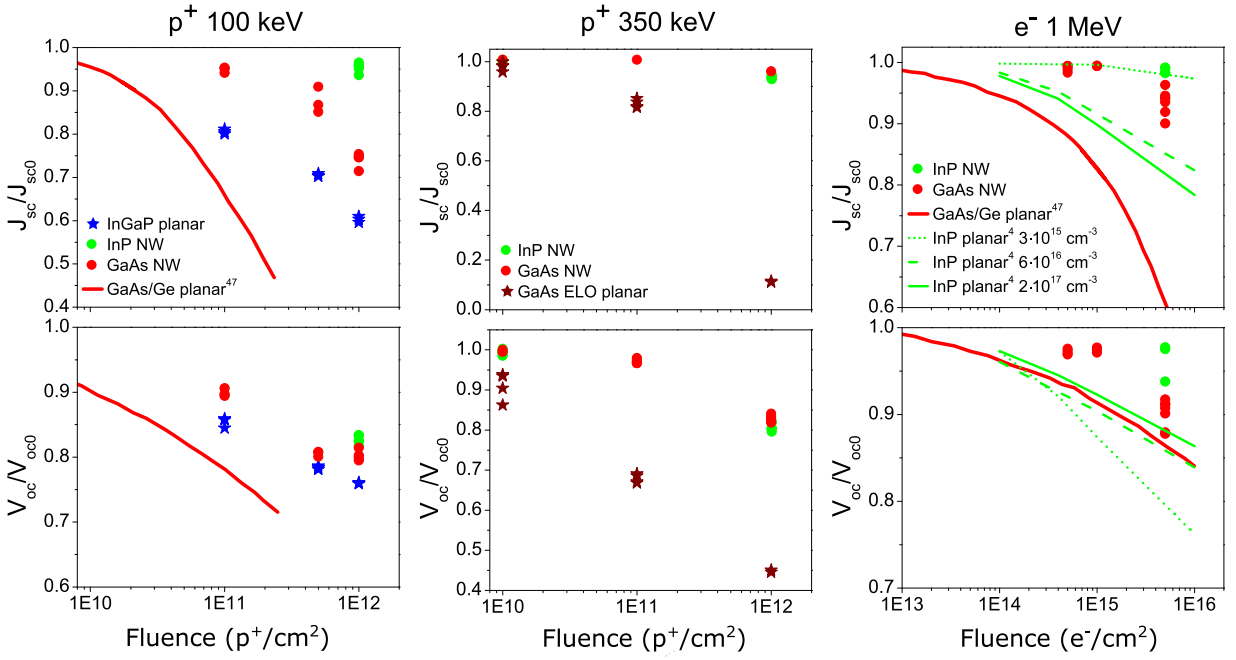

Figure 2. Solar cells performance after irradiation experiments. Degradation of the characteristic parameters (J_{sc} and V_{oc}) of different solar cells architectures tested under irradiation with 100 keV p^+ (left panels), 350 keV p^+ (center panels), and 1 MeV e^- (right panels). The points show the performance of the different solar cells included in each test. Data for the degradation of planar GaAs/Ge solar cells (red lines)[47] and for planar InP solar cells (green lines)[4] have been included for comparison.

nuclei, producing ionization and atomic displacements (vacancies and interstitial defects) in the crystal lattice that degrade material performance primarily by generation of nonradiative recombination centers. Particles with sufficient energy to completely penetrate the active region of the solar cell produce a roughly uniform damage concentration along their path.[46] However, particles with lower energies that come to rest inside the solar cell create an inhomogeneous defect distribution. In the case of electrons, the displacement rate (displacement/cm) decreases gradually as they are slowed down in the semiconductor. Protons exhibit the opposite behavior; as their energy decreases, the displacement rate increases dramatically, producing a highly nonuniform defect profile wherein most of the damage is concentrated near the end of the proton trajectory.[46] Shielding is primarily used to reduce the fluence of these highly damaging low-energy protons.[46] Therefore, any solar cell technology which aims to eliminate or to reduce drastically the shielding without compromising the service life of the solar array needs to be resistant not only to the radiation of high energy particles that penetrate the entire device but also to lower-energy particles (mainly protons) with shorter penetration depth.

To evaluate the radiation hardness of NW solar cells, we irradiated GaAs and InP NW solar cells with protons at energies of 100 and 350 keV and electrons at 1 MeV energy. The initial efficiency under terrestrial spectrum (AM1.5G) for the GaAs NW solar cells was ~11.6% ± 0.9% and for the InP NW solar cells was ~6.5% ± 0.9%. The GaAs NW cells had a wire length of 3−3.2 μm, whereas the InP NW cells had a wire length of 1.7−2 μm. The GaAs NW cells had wire core radii of ~80 nm and the InP NW cells of ~90 nm. As experimental controls, we also included 4.4 μm thick ELO GaAs planar solar cells and ~1.3 μm thick InGaP cells. The cell geometries, representative cross sectional images, and $J-V$ curves before the irradiation tests are depicted in Figure 1. Although the InP NW solar cells have moderate efficiencies, the performance of GaAs NW solar cells is comparable to that of the planar ELO GaAs solar cells. However, it should be noted that the planar devices do not have antireflective coatings; thus, a ~30% increase in current density could be expected for both the GaInP and GaAs planar cells if such a layer was used.

Performance degradation was evaluated in terms of the short circuit current density (J_{sc}) and open circuit voltage (V_{oc}), as shown in Figure 2. A summary of the devices included in each test, their initial characteristics and their performance after the irradiation is presented in Table S.1 in the Supporting Information (SI).

First, we analyzed the results of irradiation with 100 keV protons (left column panels in Figure 2), which have a short penetration depth (~750 nm), such that the ions are implanted inside all of the tested devices. The degradation as a function of fluence (degradation rate) for both J_{sc} and V_{oc} for our GaAs NW solar cells is lower than for the reference planar InGaP solar cell even though the InGaP is known to be a more radiation-tolerant material than GaAs.[3] Furthermore, the GaAs NW degradation results are noticeably better than those previously reported for GaAs/Ge solar cells.[47] The J_{sc} and V_{oc} of the GaAs NW solar cells follow the degradation slope of the GaAs/Ge solar cell reported by Anspaugh but shifted to a fluence ~13 times higher (see Figure S.1 in SI). Regarding the InP NW solar cells, the remaining factor of the $J_{sc} > 0.95$ after 1×10^{12} p^+/cm^2 is notable in comparison with the degradation of standard space GaAs/Ge solar cells.[47] For InP NW cells, the open circuit voltage degradation with irradiation is similar to that for GaAs NW solar cells. However, due to the lower initial V_{oc} in the InP NW cells, the radiation resistance of the V_{oc} should be interpreted cautiously. Future improved InP NW structures with higher V_{oc} could have a different radiation resistance.

We also analyzed results of cell irradiation with 350 keV protons (middle panels in Figure 2), which have a penetration

DOI: 10.1021/acsnano.9b05213
ACS Nano XXXX, XXX, XXX−XXX

depth of ~2.4−2.9 μm. This is close to the full length (~3−3.2 μm) of the GaAs NWs in our solar cells and we therefore would expect the protons to cause significant damage therein as well as in the thin film GaAs planar ELO devices (~4.4 μm thick). In the InP NW solar cells (~1.2−1.7 μm long), the protons cross the semiconductor structure. We found that the GaAs NW solar cells can withstand a fluence ~40 times higher than planar devices (see Figure S.1 in SI). In particular, the short circuit current density degradation ratio (J_{sc}/J_{sc0}), exceeds 0.90 at the highest fluence 1×10^{12} p^+/cm^2 in the GaAs NW solar cells, which is comparable to that of InP NW cells, and 9-fold times better than the short circuit current density degradation ratio in the planar GaAs solar cells ($J_{sc}/J_{sc0} \sim 0.1$), which are severely damaged. Likewise the degradation of V_{oc} in the GaAs NW solar cells ($V_{oc}/V_{oc0} > 0.80$) is 1.8 times lower than the planar thin film GaAs solar cells tested.

Finally, we analyzed the results of irradiation with electrons of 1 MeV (right-hand panels in Figure 2), which penetrate around ~700 μm in the semiconductor, and consequently cross the entire solar cell in all devices. We found that the J_{sc} in the GaAs NW solar cells does not change when increasing the fluence up to 1×10^{15} e^-/cm^2 (equivalent to ~15 years in geostationary orbit) and only decreases slightly ($J_{sc}/J_{sc0} \sim 0.90-0.96$) after 5×10^{15} e^-/cm^2, which indicates exceptional tolerance to electron irradiation[3] in comparison with previously reported data for various planar space GaAs solar cell architectures[47,48] where a short circuit current density degradation ratio (J_{sc}/J_{sc0}) between 0.6 and 0.85 was observed at 5×10^{15} e^-/cm^2. Also, the V_{oc} of the GaAs NW solar cells is unchanged at low and medium fluences. However, we observe an abrupt drop at the highest fluence, showing a similar degradation V_{oc}/V_{oc0} as seen in planar GaAs devices. Unlike the protons, the 1 MeV electron degradation curves of the planar and NW solar cells do not have the same shape which might indicate a different nature of the defects introduced in both architectures.[49] The InP NW solar cells also have lower degradation than previously reported values for different designs of planar InP solar cells[4] (green lines in the right-hand panels in Figure 2). A similar low short circuit current degradation rate has been reported for a planar InP solar cell with a very low-doped base. However, the V_{oc} degradation of the planar devices with a low-doped base was significant, $V_{oc}/V_{oc0} = 0.81$, in contrast to the InP NW-based devices where the degradation was almost negligible, $V_{oc}/V_{oc0} > 0.94$. The initial V_{oc} of the InP NW solar cells is low (620−660 mV) so the radiation resistance advantage should be corroborated in more advanced devices with higher initial V_{oc}.

These results suggest that the surfaces of the NWs, particularly the interfaces between the InP NW core and the SiO_x, as well as those for the GaAs core and $Al_{0.9}Ga_{0.1}As$ shell, do not degrade significantly under irradiation by high energy particles under conditions known to degrade the performance of cells.[27,32,50] NW solar cells made of different materials (InP, GaAs), with different architectures (e.g., junction geometry, wire length), and with different initial efficiencies (~6.5% in InP NW cells and ~11.6% in GaAs NW cells) have all demonstrated that both their V_{oc} and J_{sc} are more resistant to radiation damage than their planar counterparts for both proton and electron irradiation at various energies having different penetration depths in the semiconductor. It has been reported that cells made from lower-quality materials exhibit increased radiation tolerance,[51] thus because our NW cells have lower initial efficiencies than state-of-the-art planar cells, this may be partially responsible for their improved radiation tolerance. However, at least in the case of GaAs cells, our tests include both NW and planar devices with comparable and relatively high initial V_{oc} (>0.9 V), and in all conditions tested the NW cells show a significantly higher radiation tolerance than planar devices. Therefore, collectively these results point to NW-based solar cells having superior radiation-tolerance compared to planar devices.

To understand the origin of the observed high radiation-tolerance of NW-based solar cells, we performed Monte Carlo simulations[52] based on the binary collision approximation (BCA), which simulates the interaction of ions with matter by solving the classical scattering equation between the incoming ion and the target atom. We compared proton irradiation damage in a GaAs planar cell and in a GaAs NW array, using a simplified geometry consisting of a solid GaAs cuboid 1.5 μm (width, X) × 1.5 μm (length, Y) × 3.0 μm (height, Z) for the planar solar cells, and for the NW array, an array of 9 GaAs NWs with a radius of 80 nm, a pitch of 500 nm, and 3 μm long embedded in a cuboid with the same dimensions. Two sets of NW-structures (see Figure S.2 in SI) have been simulated, the first one consists of free-standing GaAs wires in vacuum (hereafter NW_{vacuum}), whereas in the second NW-structure GaAs NWs are radially covered by a $Al_{0.9}Ga_{0.1}As$ shell 30 nm wide where the shell is enclosed with a 50 nm wide SiO_2 insulating layer and the NW array is in-filled with benzocyclobutene (BCB) making the array planar ($NW_{core-shell}$). The core−shell planarized structure resembles the experimental GaAs NW solar cells tested, whereas the freestanding NWs are a notional structure. In the simulations, we irradiated the structures with a random distribution of protons (H^+) at normal incidence to the top surface of each structure (perpendicular to the planar devices, parallel to the NW orientation for the NW-based devices). Periodic boundary conditions were assumed in all structures to reproduce an infinite array. The distributions of arsenic displacements (these are the primary defects reported on irradiated n- and p-type GaAs[49]) have been calculated. Further details on the simulation procedure are presented in Methods.

The arsenic displacements produced per incident H^+ (damage) as a function of the ion energy are shown in Figure 3a) for the planar architecture. The damage (number of displacements/ion) introduced in the planar device increases with proton energy up to ~350 keV. At this energy, protons are implanted at the bottom of the GaAs (see Figures 4 and 5) after undergoing numerous collisions in the slowdown process. At higher energies, protons cross the entire semiconductor and consequently the interactions with the GaAs atoms are drastically reduced. Figure 3b illustrates the damage ratio of the planar architecture to the NW array (left axis). The results indicate that the damage in the planar structure is noticeably higher, whereas only a small part of the ion energy is deposited in the wires of the array. The benefit of the NW architecture is particularly advantageous at the energies which produce the most detrimental effects in the planar geometry. In all cases, the free-standing NW arrays (NW_{vacuum}) exhibit the lowest damage.

Three effects can happen concurrently in the interaction of high energy protons with NW arrays: (1) some of the ions that impinge on the space between wires can leave the array without depositing their energy in the wires (particularly in free-standing NWs), (2) some of the ions that initially impinge on a wire or their secondary recoils can be scattered out of the wire, and (3) some of the ions that initially enter the array through the infilled material or their secondary recoils can be deflected toward a wire. The array geometry, the density of the different materials

DOI: 10.1021/acsnano.9b05213
ACS Nano XXXX, XXX, XXX−XXX

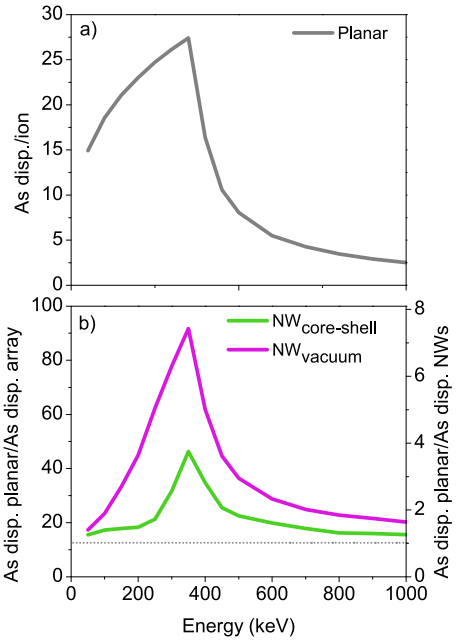

Figure 3. Comparison of the damage introduced by protons of different energies in planar and NW solar cells. (a) Arsenic displacements produced per incident ion in a planar architecture versus different proton energies. (b) Damage ratio of the planar to the NW array (left axis) and damage ratio in GaAs of the planar to the NWs (right axis).

used, and their stopping power are the main parameters which determine the distribution of the irradiation induced defects in the different layers of the NW array. On the other hand, from the viewpoint of optical absorption photons which impinge in the area between wires are absorbed because NWs have optical absorption cross sections, which are greater than their physical cross sections. Therefore, in addition to a comparison of damage (number of displacements/ion) integrated over the cuboid volume (1.5 μm × 1.5 μm × 3 μm) for the different architectures, the comparison of the damage introduced in the volume covered by GaAs has been included in Figure 3b (right axis). At all the energies and for both NW arrays (core−shell and vacuum), the ratio of As displacement/ion in planar versus NW architectures exceeds unity, confirming an effective drop in cross section for defect production in the NWs.

In order to have a better understanding of the damage features observed in Figure 3, the As displacement distributions obtained at 100 keV proton irradiation (H^+ stop near the top surface), 350 keV proton irradiation (H^+ stop near the bottom surface), and 500 keV proton irradiation (H^+ cross the semiconductor) are given in Figure 4. The induced damage per angstrom has been integrated over the solar cell thickness (*XY* plane integrated over *Z*) in the top plots of Figure 4 and over the array width (*YZ* plane integrated over *X*) in the bottom plots. The variation in the number of irradiation-induced defects in the different architectures is exhibited in the top plots. As shown in Figure 3b, the damage in the planar architecture is always higher than in the NWs and particularly advantageous is the free-standing NW configuration (NW_{vacuum}). The bottom plots in Figure 4 reveal that not only the number of irradiation-induced defects varies in the different device architectures but also their depth distribution within the cell.

The penetration profiles of irradiation-induced damage per angstrom averaged over the array area (1.5 μm × 1.5 μm, @ array) and over the NWs surface coverage ($9 \times \pi \times (80\ \text{nm})^2$, @ NW) are represented in Figure 5 for a better visual comparison. In the NW solar cells, the particle tracks in the collision cascade are truncated radially at the surfaces of the NWs, thereby reducing or eliminating the characteristic peak of induced displacements relative to that observed in bulk materials. The ions and recoils that radially leave the NWs continue the slowdown process in the surrounding material, as observed in Figures S.3. In particular, 350 keV protons are significantly scattered in the planar structure and therefore the truncation of the collisions in the NW array is markedly pronounced. The advantage of the NW array is less significant at proton energies that create a moderate number of scattering events in a planar configuration. On the other hand, the scattering events in the surrounding photovoltaically inactive material can deflect high energy particles (ions or recoils) toward the NWs. In fact, for proton energies at which all the protons are implanted in the NW array (such as 100 keV) the damage originated in the NWs by scattered high energy particles coming from the surrounding material is not negligible. In Figure 5a, two distinct regions in the irradiation-induced defect profile are observed: a first region (<750 nm) where the displacements predominantly originate via ions or recoils impinging on the NWs and a second region (>850 nm) deeper inside the wire where the displacements observed originate via collisions from scattered high energy particles that initially impacted on the surrounding material. However, as revealed in Figure 3b, the overall damage introduced in the NWs is lower than in the planar configuration.

Finally, the damage in the notional free-standing NW array simulated is even lower than in the core−shell planarized NW array. In the free-standing NWs, the ions can move undisturbed between NWs favoring larger angular and lateral spreading and ultimately enabling ions to leave the array without depositing their energy. Also, the free movement of ions between wires produces a very different defect distribution with a peak-free damage curve dispersed along the whole wire length (see Figure 5).

The energy requirements for space power systems demand lightweight, efficient, and radiation hard PV materials and devices designed for high specific power. In this study, we have assessed III−V NW solar cells for space applications by irradiation using high-energy protons and electrons and by simulating the implications of their reduced dimensions in the generation of particle irradiation-induced defects.

On the basis of our experiments, we determined that the degradation of III−V NW solar cells is significantly lower than their planar III−V counterparts for both high energy protons with a short penetration depth (100 and 350 keV) and high energy electrons (1 MeV) which cross the entire solar cells. The high radiation tolerance exhibited by the NW solar cells implies that (1) NW solar cells require less (and potentially no) shielding against low energy protons and (2) NW solar cells can potentially extend the lifetime of the mission because the unshielded high energy particles with high penetration depth are also less harmful in NW solar cells.

Because the planar and NW solar cells tested are compounds of the same III−V semiconductor materials, the irradiation results suggest that the radiation hardness of NW solar cells benefit from their array geometry and nanometric dimensions. A Monte Carlo BCA model has been used to compare proton irradiation-induced damage in a planar GaAs architecture and in a NW array resembling the device architecture of our irradiated experimental NW solar cells. The Monte Carlo BCA model

DOI: 10.1021/acsnano.9b05213
ACS Nano XXXX, XXX, XXX−XXX

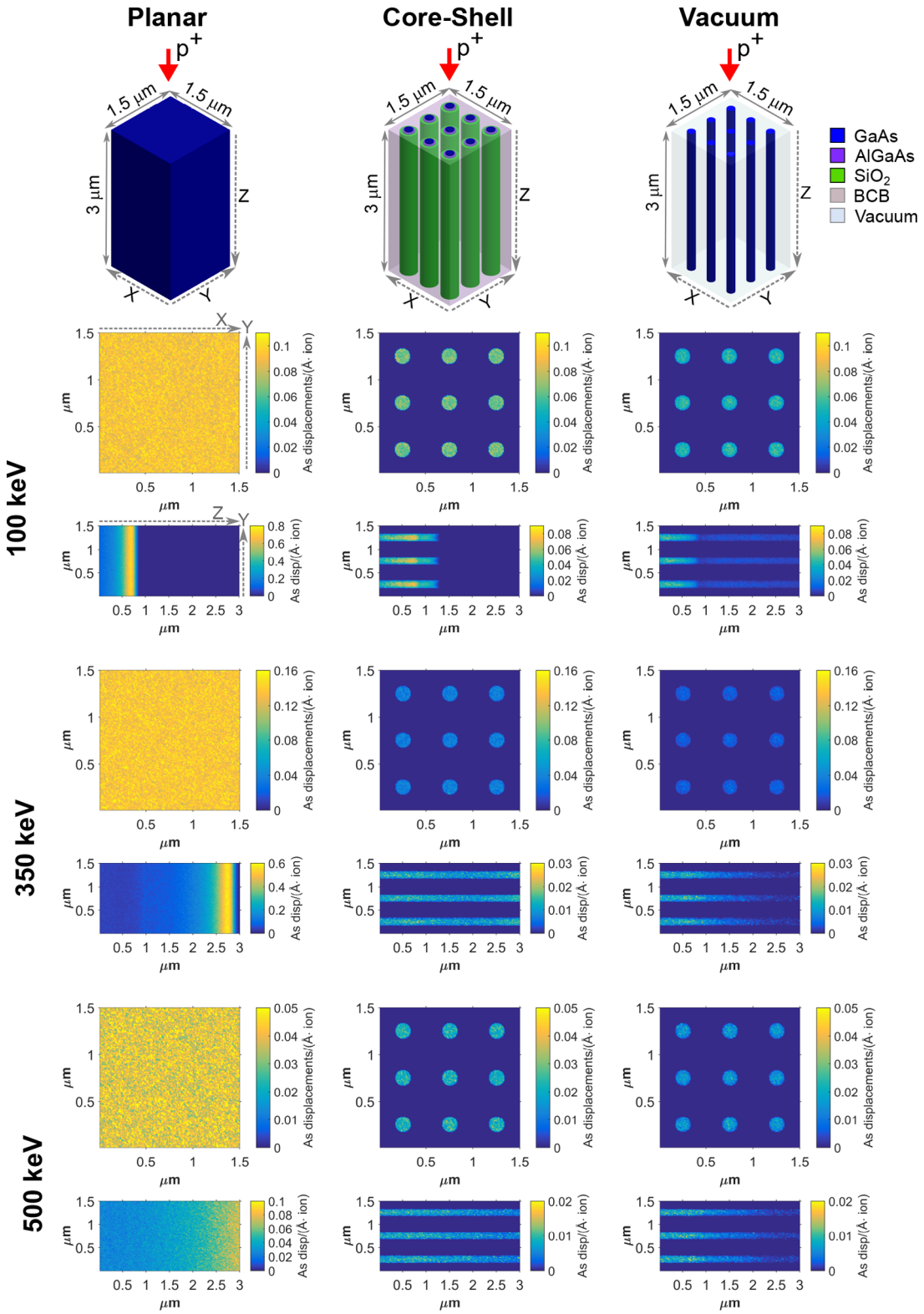

Figure 4. Damage distribution per angstrom in planar and NW solar cells after the irradiation with protons of different energies. Front view of the As displacement distribution per ion and angstrom integrated over the solar cell thickness (Z) (top plots) and lateral view of the As displacement distribution per ion and angstrom integrated over the solar cell width (X) (bottom plots) for different proton energies (100, 350, and 500 keV) and solar cell's architectures.

reveals a lower damage in the NWs than in the planar solar cells across the entire proton energy spectrum. The reduction in the irradiation-induced defect density is mainly due to the truncation of collisions in the nanometer-scale wires. Monte Carlo simulations reproduce the trend observed experimentally that the NW array configuration is particularly advantageous at proton energies that induce a large number of scattering events in planar absorber structures. As a result, the benefit of the NW

DOI: 10.1021/acsnano.9b05213
ACS Nano XXXX, XXX, XXX−XXX

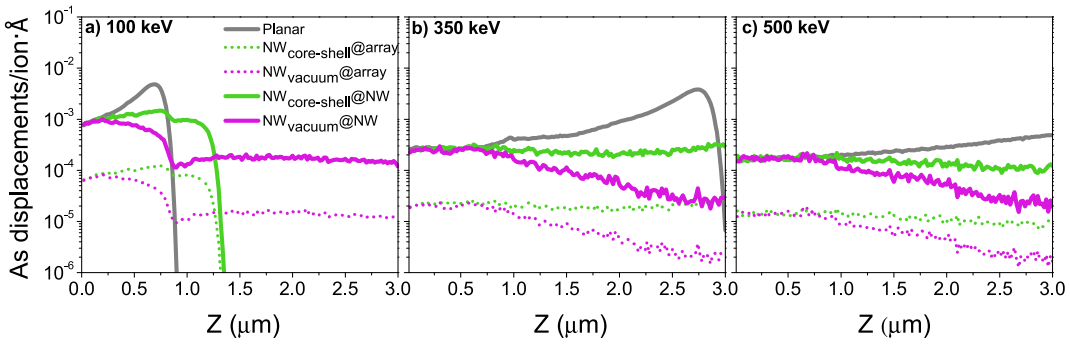

Figure 5. In-depth induced-damage per angstrom in planar and NW solar cells for different proton energies. Arsenic displacements averaged over the whole array area (@array dotted lines) and over the nanowires area (@NW solid lines) for the different device architectures and representative proton energies.

architecture is more pronounced for irradiation with 350 keV protons than with 100 keV protons. However, the radiation hardness observed experimentally is higher than the Monte Carlo BCA simulations predict. In fact, the damage ratio of the planar to the NW architecture estimated by the Monte Carlo simulations is approximately 10-fold lower than the radiation hardness observed experimentally in the irradiation tests. Monte Carlo BCA simulations model ballistic collisions of the incident ion and the generated recoils on a time scale of ∼100 fs with the target atoms assuming a temperature of 0 K. The extra energy remaining after transferring the ion kinetic energy ballistically to the target atoms is dissipated by heat conduction to the surroundings.[53] After the thermalization of the collisions on a time scale of 1−10 ps, thermally activated processes can cause the generated point defects (vacancy and interstitials) to migrate, recombine, and create defect complexes on a longer time scale[53] (nanoseconds to years). Therefore, when comparing the performance of planar and NW solar cells upon irradiation-induced defects predicted by Monte Carlo BCA simulations, the discrepancies could be due to (1) the intrinsic limitations of the simulation code to describe the production of point defects in planar and NWs architectures (n.b., the incapability of modeling the heat spike regime) or (2) other thermally activated processes[53,54] with a time scale >100 fs which play a role in transforming and reducing the residual damage in the NWs relative to that present immediately after the ballistic collision cascade. Studies of bulk GaAs show that at room temperature the intrinsic defects (vacancies and interstitials) created during irradiation can interact with previous generated defects in the crystal[49] which influences the defect migration mechanisms as well as their annihilation and accumulation. Impurities can promote the creation of stable defect complexes, whereas dislocations might act as sinks for point defects.[55] Therefore, crystal growth conditions which favor incorporation of dislocation and other defects or impurities might affect the resulting damage microstructure as it has been reported particularly in p-type GaAs.[49] The planar and the NW solar cells tested are both grown by metallorganic vapor phase epitaxy reactors (MOVPE) but at very different growth conditions and in different crystal orientations. An excellent crystal quality was observed in the transmission electron microscopy (TEM) images taken in the NW solar cells tested (Figures S.4).

Finally, it has been widely reported in the literature that the presence of surfaces/interfaces interact strongly with defects created by collision cascades.[55,56] Interfaces can attract, absorb, and annihilate defects.[57−60] Therefore, nanostructured materials with a high surface-to-volume ratio are expected to exhibit a radiation damage tolerance significantly different from bulk materials. Additionally, in the case of NWs, observation of enhanced dynamic annealing and absence of extended defects due to the dimensional confinement has been reported in Ge[61] and GaN NWs.[62] Further computational work is required to extend the knowledge of the behavior of the NW arrays under irradiation and to correlate to the electronic properties observed. In order to achieve accurate predictions, the NW array needs to be analyzed with tools which are able to model the evolution of the system from the ballistic collision until the irradiation-induced defects become immobile.[60]

However, Monte Carlo BCA simulations can only be used to make qualitative predictions; they can be used to optimize the NW array to increase the radiation hardness. In fact, Monte Carlo BCA simulations revealed that the damage in free-standing NWs is even lower. An array of free-standing NWs would behave like a planar device for light absorption but like a hollow structure for the irradiation with high energy particles.

CONCLUSION

In conclusion, III−V NW array solar cells have the potential to become efficient, lightweight, radiation-tolerant power-generating devices for space applications. In addition, because III−V NW array solar cells are made of the same semiconductor materials as standard space multijunction solar cells, they should benefit from the long heritage in development of III−V photovoltaic device technologies for space applications. Our results also indicate that further increases in radiation-robustness and specific power can be anticipated for approaches that feature (1) processing of NW devices infilled with an ultralow density mechanically stable material (such as aerogel) and (2) developing efficient substrate-free devices; this could lead to a breakthrough in the development of electronic devices for space applications.

METHODS

Solar Cells Synthesis and Fabrication. NWs were grown in a horizontal metal−organic vapor phase epitaxy (MOVPE) reactor with the vapor−liquid−solid method on (111B) substrates with predefined hexagonal or square array of Au nanodiscs with a pitch of ∼500 nm placed by nanoimprint lithography.[63] For GaAs NW growth, a p-type GaAs substrate of 5×10^{17} cm^{-3} was employed, whereas for InP NW growth a p-type InP substrate of 5×10^{18} cm^{-3} was used. Typical growth temperatures were around 450 °C at which the appropriate metal−organics are added to the carrier gas (H_2) to grow the linear n-p structures. Total lengths are 1.7−2 and 3−3.2 μm for the InP and GaAs case, respectively. Given the high aspect ratio of the semiconductor

DOI: 10.1021/acsnano.9b05213
ACS Nano XXXX, XXX, XXX−XXX

structures, special attention must be given to surface passivation. In particular, GaAs samples included an *in situ* grown AlGaAs passivation shell[31] whereas passivation of InP relied on *ex situ* oxide deposition.[32] Further details on InP and GaAs NW MOVPE growth can be found in references 32 and 31, respectively.

Samples were processed into 1.049 mm^2 solar cells in the case of the GaAs nanowire solar cells and into 0.86 mm^2 solar cells in the case of the InP nanowire devices. Details about the processing can be found elsewhere[31] but basically it consist of (1) conformal SiO_x deposition around the wires, (2) planarization of the array by spin-coating CYCLOTENE resin (Dow Chemical), (3) etch back the Au catalyst particles by selective wet etching to expose the tip of the wires, and (4) indium tin oxide (ITO) deposition top contact. Because of the small cell area, no current spreading fingers were necessary in the InP solar cells and a comblike front grid was defined with a standard photolithography process in the case of the slightly larger GaAs solar cells. In both cases, the sample back-side was glued with Ag paste to a brass coin, serving as back contact.

The planar n on p GaAs solar cells included in this study were grown inverted on top of a 5 nm sacrificial layer of $Al_{0.9}Ga_{0.1}As$ grown on a GaAs substrate. The semiconductor structure was grown in a MOVPE reactor by Spectrolab and the samples were processed into 8.41 mm^2 thin film solar cells at Caltech. Extended details about the solar cell processing can be found in ref 64 but in brief it comprises the following steps: (1) evaporation of a highly reflective back mirror which will also serve as the back contact, (2) electroplating a thick copper handle substrate (~50 μm) on top of the rear mirror, (3) bonding the copper film plated to a silicon wafer with black wax to ease the handling of the samples, (4) etch the $Al_{0.9}Ga_{0.1}As$ sacrificial layer by immersing the sample into HF/C_2H_6O (1:1) to lift-off the thin film GaAs solar cell from the thick substrate, (5) standard photolithography techniques to define the inverted square front grid contact, (6) evaporation of the front contact which consists of Pd/Ge/Au, (7) metal lift-off, (8) front contact annealing at 200 °C, (9) contact layer removal, and (10) mesa isolation by using a second photolithography step and wet chemical etching. It has to be noted that antireflecting coating (ARC) has not been deposited on the devices.

The planar n on p InGaP solar cells tested were grown and fabricated by the National Renewable Energy Laboratory (NREL). The solar cells were grown inverted by atmospheric pressure MOVPE reactor on (001) GaAs substrates miscut 6° toward (111)A as described previously.[65] After growth, the consequent processing steps were followed:[66] (1) electroplate a Au back contact, (2) bonding the samples to Si handles, (3) substrate removal via chemical etching, (4) standard photolithography to define the comblike front grid, (5) evaporation of the Ni/Au front contact, (5) contact layer removal by chemical etching, (6) second photolithography step to define the mesa etching areas, (7) wet chemical etching to isolate the devices by fully etching down the semiconductor until the Au back contact is exposed. As in the case of the GaAs ELO solar cells, ARC was not deposited on the GaInP devices.

Electron and Proton Radiation Testing. The proton testing was carried out in The Aerospace Corporation facilities in vacuum (1×10^{-6} Torr), at room temperature, the proton beam had a normal incidence on the sample, and the proton flux was 6×10^7 $p^+/cm^2 \cdot s$. The electron testing was performed in Boeing Radiation Effects Laboratory also in vacuum (3×10^{-7} Torr) at 23 °C and under normal radiation with an electron flux of 2×10^{11} $e^-/cm^2 \cdot s$.

Solar Cell Performance Characterization. The solar simulator used in the characterization before and after the irradiation tests makes use of an AM1.5G filter. In order to characterize and control the spectrum of the solar simulator, Spectrolab XTJ calibrated isotype solar cells for AM0 were used. The isotype top cell of InGaP (350−670 nm) measured ~0.5 suns (AM0) and the isotype middle cell of GaAs (500−950 nm) ~ 0.9 suns (AM0). The solar cells were measured in air at room temperature.

The initial NW solar cells efficiency under AM1.5G of ~11.6% ± 0.9% for GaAs NW solar cells and ~6.5% ± 0.9% for InP NWs reported in Results and Discussion has been obtained from the measurements in an Oriel Sol1A solar simulator with an AM1.5G filter. A Si calibrated reference solar cell was used to adjust the power of the lamp, and the measurements were carried out in air at room temperature.

Simulations Monte Carlo BCA. The evaluation of the damage distribution in the different device architectures has been carried out with the program iradina.[52] The code simulates the ion transport through the matter by means of a Monte Carlo algorithm. Similar to the well-known SRIM code,[67] iradina uses the random phase approximation, the binary collision approximation, the central potential approximation, and treats the target as an amorphous structure with homogeneous mass density. The main advantage of iradina is the possibility of simulating 3D geometries. The target structure is defined by a box divided into equally sized elementary units which account for the damage produced inside the unit, thus generating the 3D damage distribution in the defined geometry. Further details about the physics behind the model and its limitations can be found in ref 52. Here, a volume of 1.5 μm × 1.5 μm × 3 μm subdivided into elementary units of 10 nm × 10 nm × 20 nm has been simulated. Periodic boundary conditions (PBC) have been assumed laterally to mimic an infinite array. The front surface (1.5 μm × 1.5 μm) has been hit with 1 000 000 normal H^+ of different energies randomly distributed. The displacement threshold energy for Ga and As has been assumed in all the cases to be 10 eV.

ASSOCIATED CONTENT

Supporting Information

The Supporting Information is available free of charge on the ACS Publications website at DOI: 10.1021/acsnano.9b05213.

(1) Characteristic parameters of the different solar cell architectures before and after irradiation tests; (2) empirical correlation of the degradation of planar and NW GaAs solar cells under the irradiation with protons of 100 and 350 keV; (3) cross-sectional sketches of the NW structures simulated with iradina; (4) electronic energy loss distribution under the irradiation with normal incident 100 and 350 keV protons; (5) TEM images of a NW solar cell irradiated with 100 keV protons at a fluence of 10^{12} p^+/cm^2 (PDF)

AUTHOR INFORMATION

Corresponding Author

*E-mail: haa@caltech.edu.

ORCID

Pilar Espinet-Gonzalez: 0000-0002-7656-0077
Enrique Barrigón: 0000-0001-6755-1841
Giuliano Vescovi: 0000-0001-9556-0710
Alex J. Welch: 0000-0003-2132-9617
Magnus T. Borgström: 0000-0001-8061-0746
Lars Samuelson: 0000-0003-1971-9894
Harry A. Atwater: 0000-0001-9435-0201

Present Address

○(G.O.) Institute for Energy Technology, Kjeller, NO-2007, Norway.

Notes

The authors declare no competing financial interest.

ACKNOWLEDGMENTS

The authors acknowledge financial support from the Caltech Space Solar Power Project. The work performed within NanoLund was supported by the Swedish Research Council (Vetenskapsrådet), the Swedish Foundation for Strategic Research (SSF), and the Swedish Energy Agency. This research has been funded by Knut and Alice Wallenberg Foundation. This project has received funding from the European Union's

DOI: 10.1021/acsnano.9b05213
ACS Nano XXXX, XXX, XXX−XXX

Horizon 2020 research and innovation programme under Grant Agreement 641023 (Nano-Tandem) and under the Marie Sklodowska-Curie Grant Agreement 656208. This publication reflects only the authors' views and the funding agency is not responsible for any use that may be made of the information it contains. We acknowledge critical support and infrastructure provided for this work by the Kavli Nanoscience Institute at Caltech. We acknowledge the helpful contributions of J. Lloyd with the solar cell processing of the ELO GaAs solar cells at Caltech. We acknowledge The Aerospace Corporation for the irradiation test with protons and Boeing Radiation Effects Laboratory for the irradiation with electrons. This work was supported by the U.S. Department of Energy under Contract No. DE-AC36-08GO28308 with Alliance for Sustainable Energy, LLC, the operator of the National Renewable Energy Laboratory.

REFERENCES

(1) Abdelal, G. F.; Abuelfoutouh, N.; Gad, A. H. *Finite Element Analysis for Satellite Structures: Applications to Their Design, Manufacture and Testing*; Springer-Verlag: London, 2013; pp 11−47.

(2) Anspaugh, B. E. *GaAs Solar Cell Radiation Handbook*; National Aeronautics and Space Administration, Jet Propulsion Laboratory, California Institute of Technology: Pasadena, CA, 1996; pp 4-1−4-18.

(3) Yamaguchi, M. Radiation Resistance of Compound Semiconductor Solar Cells. *J. Appl. Phys.* **1995**, *78*, 1476−1480.

(4) Keavney, C. J.; Walters, R. J.; Drevinsky, P. J. Optimizing the Radiation Resistance of InP Solar Cells: Effect of Dopant Density and Cell Thickness. *J. Appl. Phys.* **1993**, *73*, 60−70.

(5) Takamoto, T.; Kaneiwa, M.; Imaizumi, M.; Yamaguchi, M. InGaP/GaAs-Based Multijunction Solar Cells. *Prog. Photovoltaics* **2005**, *13*, 495−511.

(6) Adams, J. G.; Elarde, V. C.; Hillier, G.; Stender, C.; Tuminello, F.; Wibowo, A.; Youtsey, C.; Bittner, Z.; Hubbard, S. M.; Clark, E. B.; Piszczor, M. F.; Osowski, M. Improved Radiation Resistance of Epitaxial Lift-Off Inverted Metamorphic Solar Cells. In *39th IEEE Photovoltaic Specialists Conference*; Tampa, FL, June 16−21, 2013; pp 3229−3232.

(7) Hubbard, S. M.; Bailey, C.; Polly, S.; Cress, C.; Andersen, J.; Forbes, D.; Raffaelle, R. Nanostructured Photovoltaics for Space Power. *J. Nanophotonics* **2009**, *3*, 031880.

(8) Law, D. C.; Chiu, P. T.; Fetzer, C. M.; Haddad, M.; Mesropian, S.; Cravens, R.; Hebert, P. H.; Ermer, J. H.; Krogen, J. P. Development of XTJ Targeted Environment (XTE) Solar Cells for Specific Space Applications. In *IEEE 7th World Conference on Photovoltaic Energy Conversion*; Waikoloa Village, HI, June 10−15, 2018; pp 3360−3363.

(9) Derkacs, D.; Aiken, D.; Bittner, Z.; Cruz, S.; Haas, A.; Hart, J.; McPheeters, C.; Kerestes, C.; Miller, N.; Patel, P.; Riley, M.; Sharps, P.; Stavrides, A.; Struempel, C.; Whipple, S. Development of IMM-α and Z4J Radiation Hard III-V Solar Cells. In *IEEE 7th World Conference on Photovoltaic Energy Conversion*, Waikoloa Village, HI, June 10−15, 2018; pp 3757−3762.

(10) Law, D. C.; Edmondson, K. M.; Siddiqi, N.; Paredes, A.; King, R. R.; Glenn, G.; Labios, E.; Haddad, M. H.; Isshiki, T. D.; Karam, N. H. Lightweight, Flexible, High-Efficiency III-V Multijunction Cells. In *IEEE 4th World Conference on Photovoltaic Energy Conference*, Waikoloa, HI, May 7−12, 2006; pp 1879−1882.

(11) Kayes, B. M.; Zhang, L.; Twist, R.; Ding, I.-K.; Higashi, G. S. Flexible Thin-Film Tandem Solar Cells with > 30% Efficiency. *IEEE J. Photovolt* **2014**, *4*, 729−733.

(12) Gibb, J. Lightweight Flexible Space Solar Arrays, Past, Present and Future. In *IEEE 7th World Conference on Photovoltaic Energy Conversion*; Waikoloa Village, HI, June 10−15, 2018; pp 3530−3534.

(13) Granata, J. E.; Sahlstrom, T. D.; Hausgen, P.; Messenger, S. R.; Walters, R. J.; Lorentzen, J. R.; Liu, S.; Helizon, R. Thin-Film Photovoltaic Proton and Electron Radiation Testing for a MEO Orbit. In *IEEE 4th World Conference on Photovoltaic Energy Conference*; Waikoloa, HI, May 7−12, 2006; pp 1773−1776.

(14) Woodyard, J. R.; Landis, G. A. Radiation Resistance of Thin-Film Solar Cells for Space Photovoltaic Power. *Sol. Cells* **1991**, *31*, 297−329.

(15) Lang, F.; Shargaieva, O.; Brus, V. V.; Neitzert, H. C.; Rappich, J.; Nickel, N. H. Influence of Radiation on the Properties and the Stability of Hybrid Perovskites. *Adv. Mater.* **2018**, *30*, 1702905.

(16) Miyazawa, Y.; Ikegami, M.; Chen, H.-W.; Ohshima, T.; Imaizumi, M.; Hirose, K.; Miyasaka, T. Tolerance of Perovskite Solar Cell to High-Energy Particle Irradiations in Space Environment. *iScience* **2018**, *2*, 148−155.

(17) Huang, J.-H.; Kelzenberg, M. D.; Espinet-González, P.; Mann, C.; Walker, D.; Naqavi, A.; Vaidya, N.; Warmann, E.; Atwater, H. A. Effects of Electron and Proton Radiation on Perovskite Solar Cells for Space Solar Power Application. In *44th IEEE Photovoltaic Specialists Conference*; Washington, DC, June 25−30, 2017; pp 1248−1252.

(18) Kang, S.; Jeong, J.; Cho, S.; Yoon, Y. J.; Park, S.; Lim, S.; Kim, J. Y.; Ko, H. Ultrathin, Lightweight and Flexible Perovskite Solar Cells with an Excellent Power-Per-Weight Performance. *J. Mater. Chem. A* **2019**, *7*, 1107−1114.

(19) Hirst, L. C.; Yakes, M. K.; Warner, J. H.; Bennett, M. F.; Schmieder, K. J.; Walters, R. J.; Jenkins, P. P. Intrinsic Radiation Tolerance of Ultra-Thin GaAs Solar Cells. *Appl. Phys. Lett.* **2016**, *109*, 033908.

(20) Leon, R.; Marcinkevicius, S.; Siegert, J.; Cechavicius, B.; Magness, B.; Taylor, W.; Lobo, C. Effects of Proton Irradiation on Luminescence Emission and Carrier Dynamics of Self-Assembled III-V Quantum Dots. *IEEE Trans. Nucl. Sci.* **2002**, *49*, 2844−2851.

(21) Marcinkevičius, S.; Siegert, J.; Leon, R.; Čechavičius, B.; Magness, B.; Taylor, W.; Lobo, C. Changes in Luminescence Intensities and Carrier Dynamics Induced by Proton Irradiation in $In_xGa_{1-x}As$/GaAs Quantum Dots. *Phys. Rev. B: Condens. Matter Mater. Phys.* **2002**, *66*, 235314.

(22) Kerestes, C.; Forbes, D.; Bailey, C. G.; Spann, J.; Richards, B.; Sharps, P.; Hubbard, S. Radiation Effects on Quantum Dot Enhanced Solar Cells. *Proc. SPIE 8256, Physics, Simulation, and Photonic Engineering of Photovoltaic Devices*; January 21−26, 2012; p 82561I.

(23) Bailey, C. G.; Hoheisel, R.; Gonzalez, M.; Forbes, D. V.; Lumb, M. P.; Hubbard, S. M.; Scheiman, D. A.; Hirst, L. C.; Schmieder, K.; Messenger, S.; Weaver, B.; Cress, C. D.; Warner, J.; Yakes, M. K.; Jenkins, P. P.; Walters, R. J. Radiation Effects on InAlGaAs/InGaAs Quantum Well Solar Cells. In *40th IEEE Photovoltaic Specialists Conference*; Denver, CO, June 8−13, 2014; pp 2871−2874.

(24) Anttu, N.; Xu, H. Q. Efficient Light Management in Vertical Nanowire Arrays for Photovoltaics. *Opt. Express* **2013**, *21*, A558−A575.

(25) Garnett, E. C.; Brongersma, M. L.; Cui, Y.; McGehee, M. D. Nanowire Solar Cells. *Annu. Rev. Mater. Res.* **2011**, *41*, 269−295.

(26) LaPierre, R. R.; Chia, A. C. E.; Gibson, S. J.; Haapamaki, C. M.; Boulanger, J.; Yee, R.; Kuyanov, P.; Zhang, J.; Tajik, N.; Jewell, N.; Rahman, K. M. A. III-V Nanowire Photovoltaics: Review of Design for High Efficiency. *Phys. Status Solidi RRL* **2013**, *7*, 815−830.

(27) Barrigón, E.; Heurlin, M.; Bi, Z.; Monemar, B.; Samuelson, L. Synthesis and Applications of III-V Nanowires. *Chem. Rev.* **2019**, *119*, 9170−9220.

(28) Tan, L.-Y.; Li, F.-J.; Xie, X.-L.; Zhou, Y.-P.; Ma, J. Proton Radiation Effect on GaAs/AlGaAs Core-Shell Ensemble Nanowires Photo-Detector. *Chin. Phys. B* **2017**, *26*, 086202.

(29) Tan, L.-Y.; Li, F.-J.; Xie, X.-L.; Zhou, Y.-P.; Ma, J. Study on Irradiation-Induced Defects in GaAs/AlGaAs Core−Shell Nanowires *via* Photoluminescence Technique. *Chin. Phys. B* **2017**, *26*, 086201.

(30) Li, F.; Li, Z.; Tan, L.; Zhou, Y.; Ma, J.; Lysevych, M.; Fu, L.; Tan, H. H.; Jagadish, C. Radiation Effects on GaAs/AlGaAs Core/Shell Ensemble Nanowires and Nanowire Infrared Photodetectors. *Nanotechnology* **2017**, *28*, 125702.

(31) Åberg, I.; Vescovi, G.; Asoli, D.; Naseem, U.; Gilboy, J. P.; Sundvall, C.; Dahlgren, A.; Svensson, K. E.; Anttu, N.; Björk, M. T.; Samuelson, L. A GaAs Nanowire Array Solar Cell with 15.3% Efficiency at 1 Sun. *IEEE J. Photovolt* **2016**, *6*, 185−190.

DOI: 10.1021/acsnano.9b05213
ACS Nano XXXX, XXX, XXX−XXX

(32) Otnes, G.; Barrigón, E.; Sundvall, C.; Svensson, K. E.; Heurlin, M.; Siefer, G.; Samuelson, L.; Åberg, I.; Borgström, M. T. Understanding InP Nanowire Array Solar Cell Performance by Nanoprobe-Enabled Single Nanowire Measurements. *Nano Lett.* **2018**, *18*, 3038−3046.
(33) van Dam, D.; van Hoof, N. J. J.; Cui, Y.; van Veldhoven, P. J.; Bakkers, E. P. A. M.; Gomez Rivas, J.; Haverkort, J. E. M. High-Efficiency Nanowire Solar Cells with Omnidirectionally Enhanced Absorption Due to Self-Aligned Indium-Tin-Oxide Mie Scatterers. *ACS Nano* **2016**, *10*, 11414−11419.
(34) Chen, Y.; Pistol, M.-E.; Anttu, N. Design for Strong Absorption in a Nanowire Array Tandem Solar Cell. *Sci. Rep.* **2016**, *6*, 32349.
(35) Gudiksen, M. S.; Lauhon, L. J.; Wang, J.; Smith, D. C.; Lieber, C. M. Growth of Nanowire Superlattice Structures for Nanoscale Photonics and Electronics. *Nature* **2002**, *415*, 617−620.
(36) Björk, M. T.; Ohlsson, B. J.; Sass, T.; Persson, A. I.; Thelander, C.; Magnusson, M. H.; Deppert, K.; Wallenberg, L. R.; Samuelson, L. One-Dimensional Steeplechase for Electrons Realized. *Nano Lett.* **2002**, *2*, 87−89.
(37) Mårtensson, T.; Svensson, C. P. T.; Wacaser, B. A.; Larsson, M. W.; Seifert, W.; Deppert, K.; Gustafsson, A.; Wallenberg, L. R.; Samuelson, L. Epitaxial III-V Nanowires on Silicon. *Nano Lett.* **2004**, *4*, 1987−1990.
(38) Bakkers, E. P. A. M.; van Dam, J. A.; De Franceschi, S.; Kouwenhoven, L. P.; Kaiser, M.; Verheijen, M.; Wondergem, H.; van der Sluis, P. Epitaxial Growth of InP Nanowires on Germanium. *Nat. Mater.* **2004**, *3*, 769−773.
(39) Heurlin, M.; Magnusson, M. H.; Lindgren, D.; Ek, M.; Wallenberg, L. R.; Deppert, K.; Samuelson, L. Continuous Gas-Phase Synthesis of Nanowires with Tunable Properties. *Nature* **2012**, *492*, 90−94.
(40) Barrigón, E.; Hultin, O.; Lindgren, D.; Yadegari, F.; Magnusson, M.; Samuelson, L.; Johansson, L.; Björk, M. GaAs Nanowire *PN*-Junctions Produced by Low-Cost and High-Throughput Aerotaxy. *Nano Lett.* **2018**, *18*, 1088−1092.
(41) Borgström, M.; Magnusson, M.; Dimroth, F.; Siefer, G.; Höhn, O.; Riel, H.; Schmid, H.; Wirths, S.; Björk, M.; Åberg, I.; Peijnenburg, W.; Vijver, M.; Tchernycheva, M.; Piazza, V.; Samuelson, L. Towards Nanowire Tandem Junction Solar Cells on Silicon. *IEEE J. Photovolt.* **2018**, *8*, 1−8.
(42) Standing, A. J.; Assali, S.; Haverkort, J. E. M.; Bakkers, E. P. A. M. High Yield Transfer of Ordered Nanowire Arrays into Transparent Flexible Polymer Films. *Nanotechnology* **2012**, *23*, 495305.
(43) Fan, Z.; Razavi, H.; Do, J.-W.; Moriwaki, A.; Ergen, O.; Chueh, Y.-L.; Leu, P. W.; Ho, J. C.; Takahashi, T.; Reichertz, L. A.; Neale, S.; Yu, K.; Wu, M.; Ager, J. W.; Javey, A. Three-Dimensional Nanopillar-Array Photovoltaics on Low-Cost and Flexible Substrates. *Nat. Mater.* **2009**, *8*, 648−653.
(44) Dai, X.; Messanvi, A.; Zhang, H.; Durand, C.; Eymery, J.; Bougerol, C.; Julien, F. H.; Tchernycheva, M. Flexible Light-Emitting Diodes Based on Vertical Nitride Nanowires. *Nano Lett.* **2015**, *15*, 6958−6964.
(45) Fountaine, K. T.; Cheng, W.-H.; Bukowsky, C. R.; Atwater, H. A. Near-Unity Unselective Absorption in Sparse InP Nanowire Arrays. *ACS Photonics* **2016**, *3*, 1826−1832.
(46) Tada, H. Y.; Carter, J. R.; Anspaugh, B. E.; Downing, R. G. *Solar Cell Radiation Handbook*; National Aeronautics and Space Administration, Jet Propulsion Laboratory, California Institute of Technology: Pasadena, CA, 1982; pp 3-1−3-153.
(47) Anspaugh, B. E. Proton and Electron Damage Coefficients for GaAs/Ge Solar Cells. In *22nd IEEE Photovoltaic Specialists Conference*; Las Vegas, NV, October 7−11, 1991; pp 1593−1598.
(48) Warner, J. H.; Messenger, S. R.; Walters, R. J.; Summers, G. P.; Lorentzen, J. R.; Wilt, D. M.; Smith, M. A. Correlation of Electron Radiation Induced-Damage in GaAs Solar Cells. *IEEE Trans. Nucl. Sci.* **2006**, *53*, 1988−1994.
(49) Pons, D.; Bourgoin, J. C. Irradiation-Induced Defects in GaAs. *J. Phys. C: Solid State Phys.* **1985**, *18*, 3839−3871.
(50) Chen, Y.; Kivisaari, P.; Pistol, M. E.; Anttu, N. Optimized Efficiency in InP Nanowire Solar Cells with Accurate 1D Analysis. *Nanotechnology* **2018**, *29*, 045401.
(51) Sharps, P. R.; Aiken, D. J.; Stan, M. A.; Thang, C. H.; Fatemi, N. Proton and Electron Radiation Data and Analysis of $GaInP_2$/GaAs/Ge Solar Cells. *Prog. Photovoltaics* **2002**, *10*, 383−390.
(52) Borschel, C.; Ronning, C. Ion Beam Irradiation of Nanostructures − A 3D Monte Carlo Simulation Code. *Nucl. Instrum. Methods Phys. Res., Sect. B* **2011**, *269*, 2133−2138.
(53) Nordlund, K.; Djurabekova, F. Multiscale Modelling of Irradiation in Nanostructures. *J. Comput. Electron.* **2014**, *13*, 122−141.
(54) Krasheninnikov, A. V.; Nordlund, K. Ion and Electron Irradiation-Induced Effects in Nanostructured Materials. *J. Appl. Phys.* **2010**, *107*, 071301.
(55) Doan, N. V.; Martin, G. Elimination of Irradiation Point Defects in Crystalline Solids: Sink Strengths. *Phys. Rev. B: Condens. Matter Mater. Phys.* **2003**, *67*, 134107.
(56) Kelly, R. A.; Holmes, J. D.; Petkov, N. Visualising Discrete Structural Transformations in Germanium Nanowires During Ion Beam Irradiation and Subsequent Annealing. *Nanoscale* **2014**, *6*, 12890−12897.
(57) Han, W.; Demkowicz, M. J.; Mara, N. A.; Fu, E.; Sinha, S.; Rollett, A. D.; Wang, Y.; Carpenter, J. S.; Beyerlein, I. J.; Misra, A. Design of Radiation Tolerant Materials *via* Interface Engineering. *Adv. Mater.* **2013**, *25*, 6975−6979.
(58) Beyerlein, I. J.; Demkowicz, M. J.; Misra, A.; Uberuaga, B. P. Defect-Interface Interactions. *Prog. Mater. Sci.* **2015**, *74*, 125−210.
(59) Beyerlein, I. J.; Caro, A.; Demkowicz, M. J.; Mara, N. A.; Misra, A.; Uberuaga, B. P. Radiation Damage Tolerant Nanomaterials. *Mater. Today* **2013**, *16*, 443−449.
(60) Bai, X.-M.; Voter, A. F.; Hoagland, R. G.; Nastasi, M.; Uberuaga, B. P. Efficient Annealing of Radiation Damage Near Grain Boundaries *via* Interstitial Emission. *Science* **2010**, *327*, 1631−1634.
(61) Koleśnik-Gray, M. M.; Sorger, C.; Biswas, S.; Holmes, J. D.; Weber, H. B.; Krstić, V. In Operandi Observation of Dynamic Annealing: A Case Study of Boron in Germanium Nanowire Devices. *Appl. Phys. Lett.* **2015**, *106*, 233109.
(62) Dhara, S.; Datta, A.; Wu, C. T.; Lan, Z. H.; Chen, K. H.; Wang, Y. L.; et al. Enhanced Dynamic Annealing in Ga+ Ion-Implanted GaN Nanowires. *Appl. Phys. Lett.* **2003**, *82*, 451−453.
(63) Otnes, G.; Heurlin, M.; Graczyk, M.; Wallentin, J.; Jacobsson, D.; Berg, A.; Maximov, I.; Borgström, M. T. Strategies to Obtain Pattern Fidelity in Nanowire Growth from Large-Area Surfaces Patterned Using Nanoimprint Lithography. *Nano Res.* **2016**, *9*, 2852−2861.
(64) Lloyd, J. V. *Optoelectronic Design and Prototyping of Spectrum-Splitting Photovoltaics*. Ph.D. Dissertation; California Institute of Technology, Pasadena, CA, 2018; pp 48−69.
(65) Geisz, J. F.; Kurtz, S.; Wanlass, M. W.; Ward, J. S.; Duda, V.; Friedman, D. J.; Olson, J. M.; McMahon, W. E.; Moriarty, T. E.; Kiehl, J. T. High-Efficiency GaInP/GaAs/InGaAs Triple-Junction Solar Cells Grown Inverted with a Metamorphic Bottom Junction. *Appl. Phys. Lett.* **2007**, *91*, 023502.
(66) Duda, A.; Ward, S.; Young, M. *Inverted Metamorphic Multijunction (IMM) Cell Processing Instructions*; National Renewable Energy Laboratory, U.S. Dept. of Energy: Golden, CO, 2012.
(67) Ziegler, J. F.; Ziegler, M. D.; Biersack, J. P. SRIM − The Stopping and Range of Ions in Matter (2010). *Nucl. Instrum. Methods Phys. Res., Sect. B* **2010**, *268*, 1818−1823.

DOI: 10.1021/acsnano.9b05213
ACS Nano XXXX, XXX, XXX−XXX